Shock Waves (2004) 13: 351–365
Digital Object Identifier (DOI) 10.1007/s00193-003-0220-3

Shock Waves

Original article

The thickness of detonation waves visualised by slight obstacles

M. Weber, H. Olivier

Stoßwellenlabor, RWTH Aachen, Templergraben 55, 52062 Aachen, Germany

Received 29 April 2003 / Accepted 20 October 2003
Published online 3 February 2004 – © Springer-Verlag 2004
Communicated by H. Grönig

Abstract. The reflection of detonation waves from slight obstacles, which hardly disturb the wave propagation, is observed by time-resolved schlieren photography. The following stoichiometric mixtures are used: pure and argon-diluted hydrogen-oxygen, hydrogen-air, acetylene-oxygen, and acetylene-air. Initial pressures are varied such that cell widths range from 1.4 up to 108 mm, which is twice the side length of the square cross-section of the tube. The trajectories of the incident and the reflected waves in the x, t-plane are used to determine lower limit values for the wave thickness. The considerable influences of the obstacle shape and of the evaluation method on the results are discussed in detail, and error sources are analyzed. The method has been improved since a previous publication by the authors. The ratio of the lower limit values to the cell width spreads from 0.4 to 0.8 in the medium cell size range. It decreases with increasing marginality and seems to increase at small scale. A unique correlation between the lower limit value and the tube diameter, both referred to the cell size, that was proposed earlier in the literature has to be refused. The velocities of the reflected waves are presented as additional information on the post-detonation wave state. The sonic transition is discussed theoretically, enhancing the stream tube model, and practically, based on detailed observations for marginal detonations.

Key words: detonation waves, sonic plane, cell size, velocity deficit
PACS: 47.40.-x

1 Introduction

The detonation wave thickness has been used by Fay (1959) to explain the deficit of the wave velocity — in respect to the Chapman-Jouguet value — that appears, when a self-sustained wave propagates in a stable way in a small tube. This deficit was found to be proportional to the stream tube area increase[1] within the finite thickness of the wave. Applying a turbulent boundary layer model, Fay found that the deficit depends on the wave thickness to a power of 0.8. As experimentally obtained values of the wave thickness differ enormously — ranging from 0.2 up to 10 times the detonation cell width λ (Dabora et al. 1965; Vasiliev et al. 1972a and b; Edwards et al. 1976; Weber et al. 2001a), more precise data are essential for the detailed understanding of velocity deficit and failure.

First of all the wave thickness has to be defined. In the classical Chapman-Jouguet model the wave is a discontinuity. If the wave is self-sustained, it is followed by an expansion wave and the C-J condition for stability is, that the post-wave gas velocity in shock fixed coordinates equals the equilibrium speed of sound. In the one-dimensional Zeldovich-von Neumann-Döring model the post shock velocity is subsonic at first and then accelerates according to the energy release to the final (sonic) state. In the final stages of the combustion the equilibrium is approached exponentially, but one might define a practical thickness similarly to the edge of a boundary layer. In Fay's *quasi* one-dimensional stream tube model the wave thickness is determined by the location where the decaying rate of energy release locally just compensates the effect of the stream tube area increase such as to allow a steady sonic transition. This can be expressed mathematically by use of the velocity area relation for reacting flow (1), whose RHS has to become zero for $M_f = 1$.

$$\left(M_f^2 - 1\right) \frac{du}{u} = \frac{dA}{A} + \frac{\Delta h^R d\alpha}{c_{p,f} T} \,. \tag{1}$$

Herein $c_{p,f}$, Δh^R and α are the chemically frozen heat capacity, the heat of reaction, and a reaction progress parameter respectively. The relation is obtained by use of the conservation equations, the caloric and the thermal equation of state, all in their differential forms, and a definition of the reaction progress parameter by its effect on the enthalpy:

Correspondence to: M. Weber
(e-mail: micha@swl.rwth-aachen.de)

[1] Viewing the wave in the steady shock fixed co-ordinate system, the flow acceleration in the wall boundary layer leads to a negative flow displacement, that causes an area increase in the core flow.

$$d(\rho u A) = 0\,, \quad dp + \rho u du = 0\,, \quad dh + u du = 0\,,$$
$$dh = \left(\frac{\partial h}{\partial T}\right)_\alpha dT + \left(\frac{\partial h}{\partial \alpha}\right)_T d\alpha\,,$$
$$\frac{dT}{T} = \frac{dp}{p} - \frac{d\rho}{\rho} \quad (\text{for const. } \alpha)\,,$$
$$\alpha = \frac{h - c_{p,f}(T - T_{CJ}) - h_{re}}{\Delta h^R}\,,$$

where the heat of the reactants h_{re} and the heat of reaction, that is negative, are evaluated at the reference temperature T_{CJ} and $c_{p,f}$ is evaluated in the C-J state. The reference sound speed for the Mach number is the one for *frozen* chemistry, which was not mentioned explicitly by Fay.

$$a_f^2 = (\gamma_f - 1) c_{p,f}\, T = \gamma_f \frac{p}{\rho}\,.$$

He determined the sonic locus by use of a simple exponential relaxation law for α. The result depends largely on this law and on the boundary layer model. In his deficit model, Fay neglected then the small fraction of energy that is released downstream of the sonic transition.

Today it is generally agreed that the C-J condition is based on the *equilibrium* sound speed (e.g. Williams 1985). The corresponding velocity area relation (2) can be obtained by use of a non-equilibrium parameter β in the differential enthalpy expression, that decays from its initial value evaluated at the von Neumann temperature down to its equilibrium value, that is zero.

$$dh = c_{p,e} dT - \Delta h^R d\beta\,, \quad \text{with} \quad \beta = \frac{h_e - h}{\Delta h^R}\,,$$
$$(M_e^2 - 1)\,\frac{du}{u} = \frac{dA}{A} - \frac{\Delta h^R d\beta}{c_{p,e}\, T}\,. \qquad (2)$$

The equilibrium enthalpy h_e is determined at the local temperature and at a reference pressure, e.g. p_{CJ}. The effect of the pressure variation during the reaction on the enthalpy is of second order only, similar to the effects of temperature and composition on c_p and R.

The parameters α and β approach their equilibrium values with similar relaxation laws and lengths. The equilibrium Mach number becomes equal to 1 before the frozen one, and limits the subsonic flow field, that is stationary within this model.

The cellular structure of real detonation waves now implies several problems: The minor, experimental one is related to the determination of the average position of the wavy leading shock front. This problem is treated in Sect. 4. The more complex one is the definition and the determination of the rearward surface of the wave. A considerable fraction of the chemical energy is first converted into hydrodynamic energy (transverse waves, longitudinal pressure waves and turbulence), or its release is delayed (unburned pockets) before it is finally transferred into enthalpy and longitudinal velocity. As this process is much slower than the approach to chemical equilibrium, it is considered as improper to define the rearward wave surface by the latter process. Soloukhin (1969) suggested instead to consider the "hydrodynamic thickness" – without exactly defining it. The dissipation process, i.e. the conversion of hydrodynamic energy, represents a similar problem as the approach to chemical equilibrium in the one-dimensional models: It is strong close to the front, but then it becomes weaker quasi-exponentially without reaching a well defined end; transverse waves for example can remain visible for a considerable time (e.g. Edwards et al. 1966, or Fig. 16). But, as for the one-dimensional models, the flow behind the real wave will undergo definitely some kind of sonic transition — provided the wave is stable and self-sustained, and the velocity deficit is not excessive. So, there must be a plane moving in a definite distance x_{ss} behind the mean front path where the *average* values of the longitudinal velocity component (in the shock frame) and of the sound speed coincide — taking the averages in time and over the cross-section of the core flow. This plane may be called **s**hock-frame **s**onic plane (ss) and it determines the wave thickness. In analogy to Fay's model it should be located where the decaying average of the energy transformation correspondingly matches the effect of the average area increase. In the authors' opinion the expression "sonic plane" (as just defined) should be distinguished from the expression "sonic surface", which may refer to the instantaneous set of sonic points. To our knowledge this distinction has not been made so clearly yet. The fluctuating sonic surface can be curved and even discontinuous due to the action of transverse waves or longitudinal pressure waves, and these attributes are pronounced at initial conditions close to the limit of propagation. The mean location of the sonic surface does not have to coincide precisely with that of the sonic plane.

Furthermore it is suggested, that in an improved quasi-one-dimensional flow model, the enthalpy should contain not only thermal and chemical energy, but also the hydrodynamic energy from transverse waves and turbulence, so that the equation $dh = -u du$ of the simple, quasi one-dimensional model is still applicable. Then α and β respectively describe the whole process of energy transformation — not just the chemical reaction.

It has been a subject of discussion, whether the strong fluctuations in marginal regimes would allow a penetration of disturbances through the sonic plane in the upstream direction. To approach this question, one may consider a very strong fluctuation that may change the instantaneous shock frame flow velocity in an arbitrary point of the sonic-plane periodically between 0.9 and 1.1 times the mean sound speed, and the instantaneous sound speed vice versa, both being average values for the subsonic and the supersonic period of time respectively, so that the flow Mach number switches between 0.82 and 1.22 correspondingly. The characteristic time of the fluctuation λ/a_{ss} is determined by the mean distance of the dominant transverse waves λ, that cause or accompany the most important flow phenomena and that move at a velocity of about a_{ss}. A small disturbance may propagate upstream starting at the sonic plane, when half of the subsonic period has passed (Fig. 1). It will move with a net Mach number of 0.18 for the second half of it and cover a distance

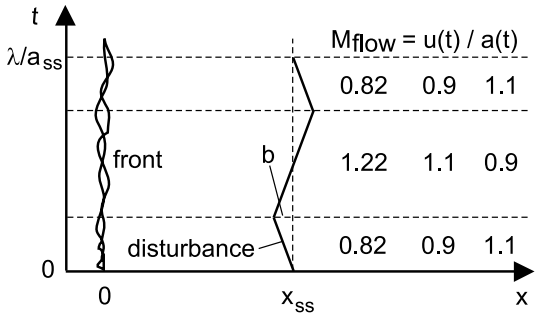

Fig. 1. Path of a disturbance generated in the sonic plane at $t = 0$ watched in a shock-fixed frame at given velocity changes, $b = (1.1 - 0.9)a_{ss}\lambda/(4a_{ss}) = 0.05\lambda$

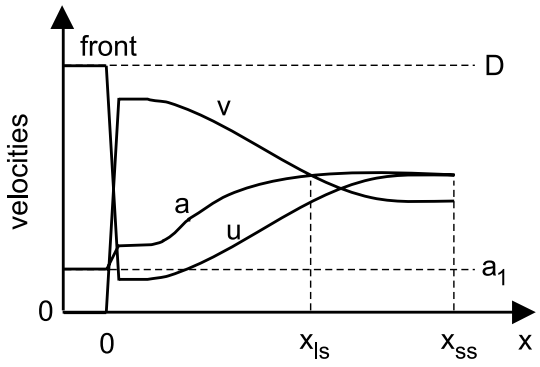

Fig. 2. Shock frame velocity u, laboratory frame velocity v, and speed of sound a in a one-dimensional detonation wave model

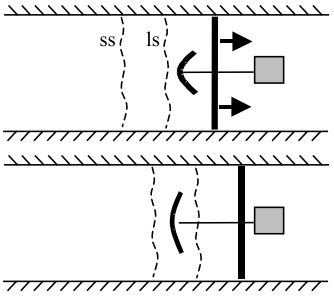

Fig. 3. Detonation wave reflection from a thin obstacle

$b = 0.05\ \lambda$, before it will be pushed back behind the sonic plane to the same amount in the supersonic period. As the wave thickness is definitely very much larger than b, it is unlikely that the disturbance will have any influence on the front. As well it is unlikely that it "climbs" upstream from one subsonic region to another, temporarily neighbouring each other, because any transversal movement of a wave is accompanied by a reduction of the longitudinal component of propagation. No expansion and no small compression generated some distance downstream of the sonic plane is capable to reach the front; it will always fall behind. Therefore, the concept of a sonic plane as defined above should be applicable even in stable marginal regimes.

To determine the location of the sonic plane, various experimental methods have been used in the past. Edwards et al. (1976) measured the decay of pressure oscillations and obtained x_{ss} to λ ratios ranging from about 2 up to 4. Dabora et al. (1965) studied detonation wave propagation in a rectangular channel, where the detonative gas was unilaterally bounded by nitrogen - separated by a 25 nm thin nitrocellulose film. They photographed the deflection angle of the combustion products, adapted Fay's stream tube model, and obtained a wave thickness of 2.8 mm for stoichiometric oxy-hydrogen at atmospheric pressure, which yields $x_{ss}/\lambda \approx 1.75$. Fay himself had inferred a thickness of 3.5 mm. Vasiliev et al. (1972) used two different optical methods, one of which was analogous to Dabora's method, just that a cellophane tube completely surrounding the mixture was used. They obtained x_{ss}/λ values ranging from 3.6 for oxy-hydrogen up to 10 for acetylene oxygen. The velocity deficits, measured with an accuracy of only 50 m/s, were used to calculate the relative area increases (about 0.02). The corresponding location was then measured in the photographs. The surface density of the tubes was 0.005 g/cm^2, corresponding to a thickness of about 36 μm, which was 1500 times as much as in Dabora's experiments. Following Dabora already due to their weight such thick films would hinder the immediate lateral expansion of the products, which can be a reason for the large values of the results.

With their second method, Vasiliev et al. (1972a) aimed at the location of the lab-frame sonic surface (index ls) as a lower limit for the shock-frame one (ss), which is possible because the lab-frame velocity in the C-J state is slightly subsonic for common gaseous mixtures ($Ma \approx 0.8$ to 0.9). Figure 2 shows the evolution of the average velocities within the wave. In their experiments, the edge of a thin plate faces the approaching detonation as a slight obstacle (Fig. 3). As soon as it is engulfed by the front, a weak oblique shock forms in the initially supersonic flow (lab frame). When the flow becomes subsonic, the shock slowly starts to move upstream. The obtained values for the ratio of the wave thickness to the cell size decreased with increasing cell size from 3 (for $\lambda = 0.7$ mm) down to 0.3 (for $\lambda = 30$ mm, Vasiliev et al. 1972b).

Murray and Lee (1986) correlated the deficits occurring in tubes with yielding walls to the observed expansion ratios that are reached *one cell length* behind the front. This length measure was chosen arbitrarily such that the deficit prediction using Dabora's version of Fay's stream tube model consisted with the (strongly scattering) measured deficits. With similar success it was used to correlate the rigid tube results of other authors, calculating the expansion ratios with Fay's displacement thickness expression. Cell lengths were taken to be $\lambda/0.7$, and λ was calculated with various correlations based on experimental results obtained at conditions far from the limit.

Murray and Lee did not observe a change of the cell size with increasing velocity deficit in the yielding wall tube, in spite of the decreasing post-shock temperatures and reaction rates. This is in contrast to observations in (small) rigid tubes and channels, where the cell size exceeds clearly the natural (large tube) value (e.g. Weber

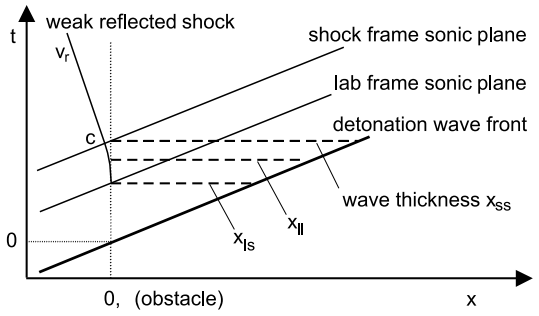

Fig. 4. Detonation wave reflection from a slight obstacle (average velocities, one-dimensional)

et al. 2001b; Vasiliev et al. 1972b). Therefore the real deficit should become larger. Unfortunately the large scatter of the experimental velocity deficit data found in the literature (e.g. Murray and Lee 1986; Auffret et al. 2001) does not allow the verification of further refined deficit models. Nevertheless, the determination of the wave thickness is of general interest and will allow a closer look to the physics. The authors consider Vasiliev's second method as promising, because it deals directly with the velocities.

Figure 4 shows the reflection of a detonation wave from a small obstacle in the x,t-plane based on averaged velocities, for initial conditions far from the propagation limits. The path of the detaching weak shock is curved initially and adopts finally a nearly constant velocity, which is observed in Weber et al. (2001a) and in this work. The effect of the Taylor expansion is negligible for usual long detonation tubes. At conditions closer to the propagation limits the relative area increase per unit length is large, so that according to Eq. (2) also the energy conversion rate in the sonic plane has to be still large for that the RHS equals zero. Due to both effects the acceleration of the weak wave must continue into the (shock frame) supersonic region to a small extend, which is is not yet verified experimentally. Magnitude and behaviour of the acceleration depend on the boundary layer and on the relaxation (energy conversion), which are both not thoroughly investigated so far - while Fay assumed a turbulent boundary layer, Hartunian et al. (1960) observed a laminarisation of boundary layers for high heat transfer rates. Additionally, there are difficulties for the *experimental* determination of the course of the acceleration:

- the presence of the fluctuations, of the shock position uncertainty $\Delta x_{r'}$ and of a limited temporal resolution, that calls for a large number of experiments,
- the decaying strength of the shock (for single obstacles), that fades away with increasing distance from the obstacle, and
- the dispersion of a weak wave into a step-wise front of decreasing strength, that propagates at a_f, and a smooth main effect of increasing strength, that propagates at a_e (Vincenti and Kruger 1967). It is not clear which effect is visualized here.

Due to these difficulties of prediction and measurement, so far it is only possible to determine a lower limit for the location of the shock frame sonic plane.

2 Details of the measurement principle and accuracy estimates

Evaluating several experiments at a framing frequency of 1 MHz, Vasiliev determined the separation time as the moment when the apparent downstream edge of the shock clearly separates from the plate. This moment is influenced by the apparent thickness of the shock, that depends on the optical system (blur), on the schlieren sensitivity, and on the waviness/curvature of the reflected shock. The portion that is due to optical reasons is independent of the size of the structure studied, so that the relative lower limit value becomes increasingly over-estimated with decreasing scale. To avoid this influence, here, the positions of the apparent *centers* of the reflected shock are plotted in an x,t-diagram, and a best fitted straight line is drawn through them disregarding those first points that clearly deviate from the line. It is extended to the position of the obstacle tip to obtain the separation time t_s, which is then multiplied by the mean wave speed to obtain x_{ll} (Figs. 4, 10, 14). This value is mostly somewhat smaller than Vasiliev's and smaller than the wave thickness x_{ss} but larger than the distance from the front to the *lab-frame* sonic plane x_{ls}. So it yields a reasonable lower limit value. The obtained velocity of the reflected shock v_r provides information about the post-detonation wave state. The so determined separation time is influenced by the judge of the investigator, i.e. by his choice of the first point to be incorporated into the linear fit. A general guideline for this choice, that is applied in this work, is to maximize the expression

$$F = \frac{v_r(n'-1)}{1+10\sigma_r/x_{ll}}\,, \tag{3}$$

where $n' = \sum \psi_i$ is the weighted number of all incorporated points, with ψ_i being a weighting factor used in the linear regression, which is usually 1 but is set to a value smaller than 1 (mostly 0.25), where the reflected shock is badly visible or strongly blurred. This expression becomes larger with the number of included points till the determined velocity v_r decreases and the standard deviation σ_r increases. It is not meant to be thoroughly reasoned, but describes the decisions of the first author, so that they can be reproduced by others. For much higher temporal resolutions other guidelines would have to be chosen.

The accuracy of the determined lower limit value x_{ll} depends on the accuracy of the velocity determination Δv_r, on the blur of the obstacle tip as it appears in the image Δx_0, and on the determination of the mean front positions Δx_f. The corresponding errors can be cumulative so that the maximum possible error of the lower limit value Δx_{ll} becomes

$$\Delta x_{ll} = |\Delta v_r|\, D\, \frac{x_0 - x_m}{v_r^2} + |\Delta x_0| \left(1 + \frac{D}{v_r}\right) + |\Delta x_f|\,, \tag{4}$$

being D the detonation wave velocity and x_m the mean position of all x,t-points incorporated in the linear fit, which is determined by $x_m = \sum(\psi_i x_i)/\sum \psi_i$. The error of the velocity measurement Δv is a purely statistical one.

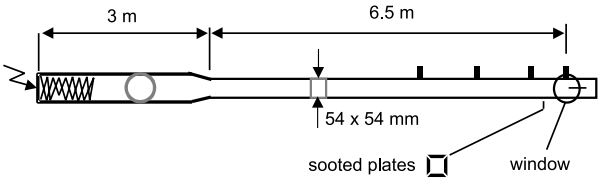

Fig. 5. Set-up of detonation tube facility Q54

For a worst case error estimate Δv_r, it is assumed that all shock positions on the left of x_m are mis-estimated by $\Delta x_r \psi_i^{-1/2}$ to one side and all the others to the other side, which gives

$$\Delta v_r = \Delta x_r \frac{\sum_i |t_i - t_m| \sqrt{\psi_i}}{\sum_i (t_i - t_m)^2 \psi_i} \qquad (5)$$

with the assumed general uncertainty of the shock position $\Delta x_r = (1.5 + 2\lambda/d)$ pixel, that includes a roughly estimated effect of the fluctuations, with d being the tube diameter. The small uncertainty of the exact obstacle position Δx_0 has an amplified influence on x_{ll}, which is easily understood by a lateral shift of the vertical line (obstacle position) in Fig. 4. The uncertainty for the front position Δx_f is described in Sect. 4. The latter two error sources have statistical and systematic causes. They are present in Vasiliev's method as well, whereas the above mentioned source for systematic errors of his method is replaced here by the statistical error Δv_r, which is less harmful. Additional error sources related to the obstacle shape and arrangement are discussed in Sect. 5.

3 Experimental set-up and conditions

The detonation tube is shown in Fig. 5. Detonation initiation is facilitated by a highly explosive mixture at the ignition end, that is filled in just before the shot, occupying about 10 % of the tube volume. It is ignited by a spark plug. The nitrogen/oxygen ratio in the air in use is 79.5/20.5. The wave velocity and its stability are measured by four piezo-electric pressure gauges, located at distances 7, 707, 1707 and 2707 mm in front of the obstacle, and the cellular structure is recorded by four sooted plates. For small cells thirty triple-point traces along some arbitrarily chosen lines are evaluated. For large cells the soot traces of all the four plates are evaluated, dividing the double of the perimeter by the number of traces. For the fuel-air mixtures in the marginal regime only dominant traces are taken into account; in the normal regime substructures have not been identified, so that all visible traces are evaluated. The results of these measurements are presented in Fig. 6. Velocities are deduced from linear fits through the signals of first three gauges. Chapman-Jouguet velocities are calculated with STANJAN (Reynolds 1986).

The velocity deficit increases with decreasing pressure as qualitatively expected. For the two experiments with hydrogen-oxygen that yielded a detonation velocity slightly above the C-J value a slightly too large hydrogen

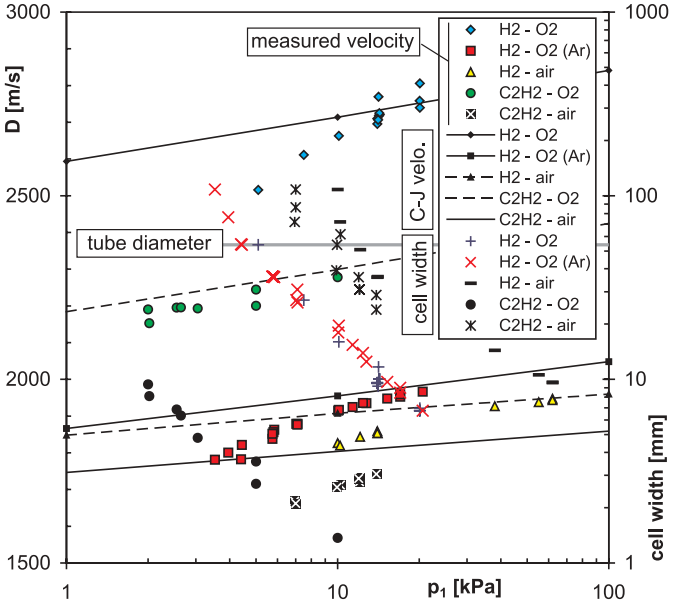

Fig. 6. Detonation wave velocities and cell widths in stoichiometric mixtures (volume fraction of Ar is 40 %)

fraction in the mixture can be supposed (plate experiments in Fig. 20). Towards the test-section a slight deceleration of the wave was observed: a second order curve fit through all 4 gauge signals using the least squares method gave final velocities that were in the mean 1.5 % smaller than the presented linear fit values. This deceleration was probably due to an unidentifiable small leakage. Its impact on the wave thickness is supposed to be much smaller than the general measurement errors discussed before. It has been checked by use of a fifth pressure gauge mounted 150 mm downstream of the conical section of the tube, wether the deceleration could be the effect of a slow re-equilibration of the wave after the overdriven state occurring in the cone, but this was not the case. The equilibration takes place so quickly, that the mean wave speed on the first half of the square section, does not differ significantly from that between the following three gauges.

The measured cell sizes (< 54 mm) agree well with published data. Pure oxy-hydrogen values exceed the data of Strehlow (1969), but to a lesser amount than the data of Desbordes (1990) and Zitoun et al. (1995) in the 20 to 40 kPa range. The values of argon-diluted oxy-hydrogen fit the data of Barthel (1974) exactly. The acetylene-oxygen data of Edwards et al. (1978), Desbordes (1988) and Laberge et al. (1993) are matched as well. The cell widths measured in hydrogen-air are about 80 % of the cell lengths given by Bull et al. (1982). This ratio should be slightly smaller, but the difference is within the common uncertainty for hydrogen-air. The cell widths of acetylene-air fit those calculated from the work of Bull. For argon-diluted hydrogen-oxygen and for hydrogen-air the slope of the cell sizes becomes steeper as the tube side length is passed (see Fig. 6). Cell widths of 108 mm correspond to a rectangular-mode detonation structure, where only one triple point trace appears on each of the four sooted

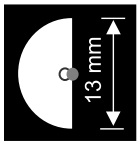

Fig. 7. Schlieren edge and laser focus positions

plates. These traces culminate in typical slapping wave marks on the neighboring plates, and the orientation of opposite triple-point traces is equal, so that there are two transverse waves - one in each orientation. Spinning mode did not occur.

For the time-resolved schlieren photography a ruby-laser stroboscope and a rotating-mirror camera are used together with spherical mirrors of 2 m focal length in a standard arrangement. A semi-circular schlieren edge was used with the laser focus set close to the vertical knife (Fig. 7) yielding a high sensitivity and cutting off the light deflected by the reflected weak shock and by the reaction zones with a high sensitivity. Leading shock waves deflect the light so much that it leaves the semicircle. At low pressures the focus is centered on the knife edge to increase the sensitivity even more. In this case, leading shock waves that are curved or oblique to the optical axis appear whitish. They can appear black, where they are planar and parallel to the optical axis, i.e. the integrated schlieren effect is high. The framing frequency was varied between 0.2 and 1 MHz by adaptation of the object size. The relative film speed was 2.1 mm/μs. For post-processing the film was scanned at a resolution of 2700 dpi yielding a resolution of 18 pixel per millimeter of the test-section.

Three kinds of obstacles have been used, a thin plate consisting of two razor blades that are glued together, rakes of sharp needles and planes of bluntly wedged needles, that are wider spaced than in the rakes and cover the whole cross-section of the tube (Fig. 8). A single row of needles with 2 mm spacing did not produce any schlieren effect, but the double rake did and the short triple rakes as well.

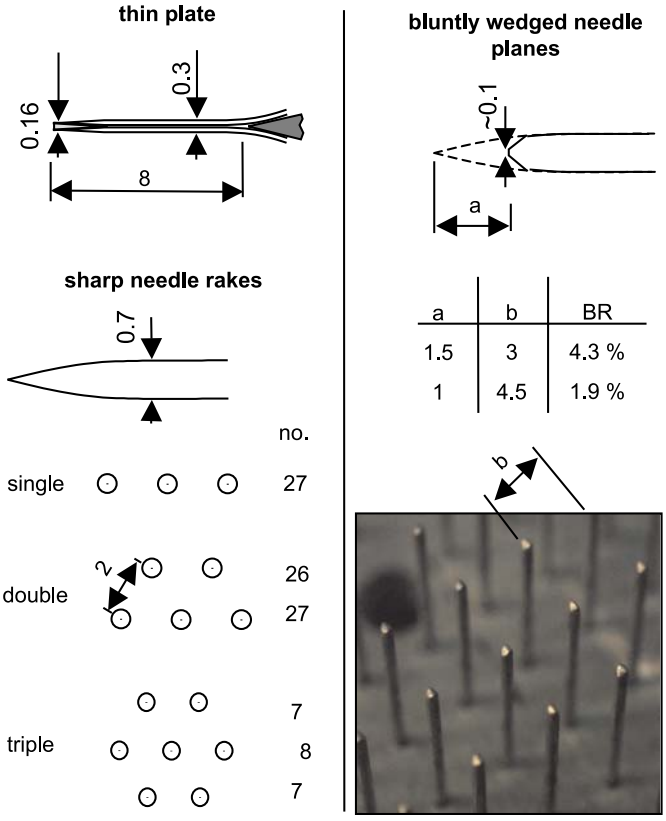

Fig. 8. Obstacle geometries and arrangements (dimensions in mm, BR = blockage ratio)

4 Details of the image evaluation

The digital frames are rotated and carefully arranged on the canvas using a reference object. Care has to be taken, because strong density gradients in the vicinity of edges can influence their apparent position. If the obstacle tip appears sharply it is used as reference till the front arrives, then the right border of the window is used and at last the left one. The error in positioning is about $\pm$ 0.5 pixel. It is part of the above mentioned uncertainty of the shock position Δx_r. The blur of the obstacle tip, as that of all edges, becomes larger with increasing schlieren sensitivity. The position of the obstacle tip x_0 and its uncertainty Δx_0 are estimated by comparison with images taken at low sensitivity without flow.

The arrival time of the front at the obstacle is determined in the x,t-plane by the moment when the best fitted straight line through the front positions x_f, given by as many frames as possible, passes the obstacle position. This is done for two reasons: first, for a limited temporal resolution the exact instant of the first contact with the obstacle will rarely be captured by a frame, and second, the moment of shock detachment is influenced by the whole flow field, which follows the mean path of the front. Unfortunately, the mean front position defined as

$$\overline{x_f} = \frac{1}{A} \int_A x_f dA \,,$$

where A is the cross section of the tube, cannot be determined from a usual photograph. So, a practical value has to be defined. In this work the rearmost point on the foremost front line visible in the image plane is chosen (circles in Fig. 9), because at the same time this point is the foremost point on its front line in the horizontal plane. The true value will be mostly mis-estimated, but in both senses, so that the single errors are equilibrated by the linear fit. Unfortunately, the degree and frequency of relative over-estimation increases with the number of cells in the line of sight, if the structure is not extremely regular, because the wave crests obscure the troughs more and more. A correction would only make sense, if data about the waviness, that depends on λ/d, was available. The data of Weber et al. (2001a) has been corrected according to the present method and is included in Fig. 21.

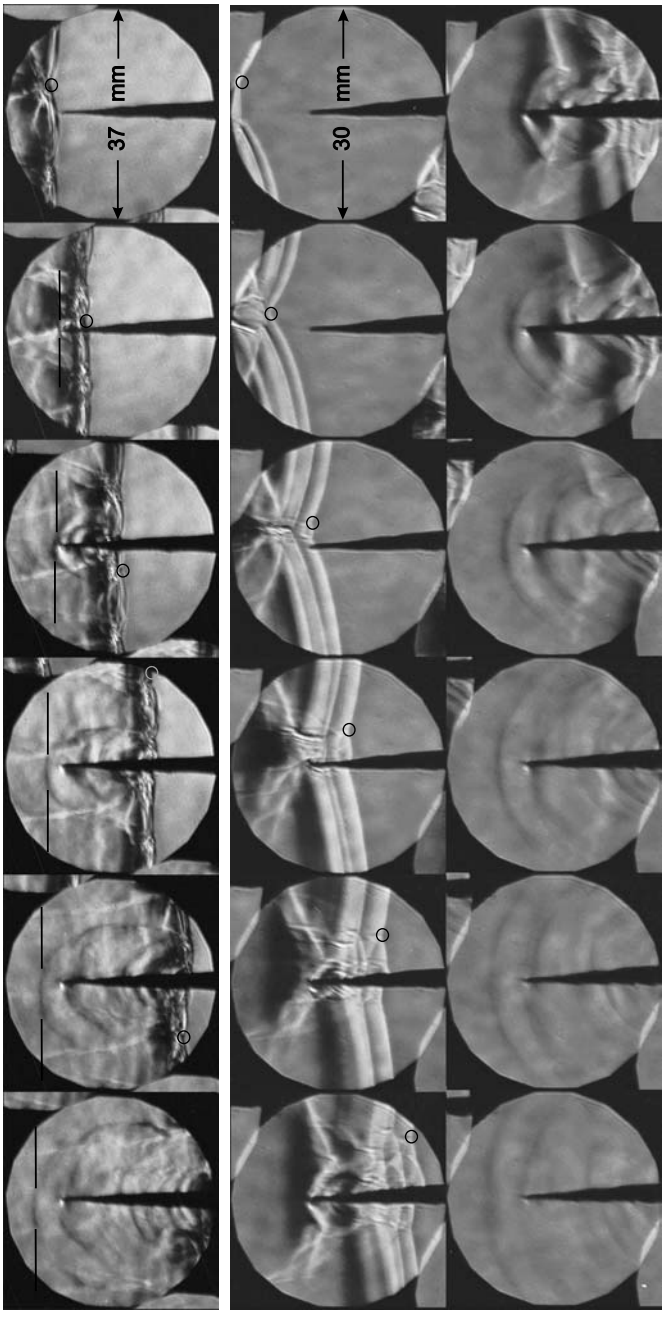

Fig. 9. Estimates of front positions (O) and reflected shock positions (|) in $2H_2 + O_2 + 2Ar$. Left column: $\Delta t = 3$ μs, $p_1 = 12.4$ kPa, $\lambda = 13$ mm. Middle and right: 2.5 μs, 4.4 kPa, $\lambda = 54$ mm

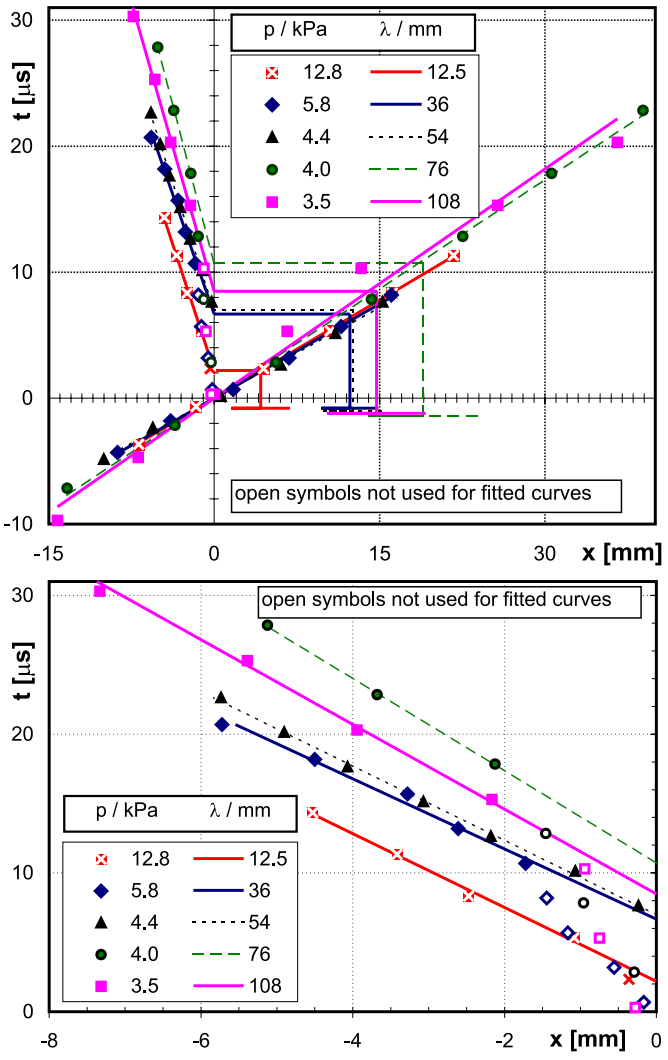

Fig. 10. Reflection of detonation waves at the plate. Determination of lower limits of the wave thickness x_{ll}, with maximum error estimates. Enlargement: reflected waves ($2H_2$+O_2+2Ar)

5 Influences of the obstacle shape and arrangement

Figure 10 shows the paths of detonation waves reflecting from the thin plate for five experiments at low initial pressures. The wave thickness is not determined by the detonation wave velocity from the schlieren images, which is not very accurate due to the short observation length, but by the more exact one given by a linear fit through the arrival times at the last three gauges in front of the obstacle. The points shown by triangles correspond to the frames of the medium and the right column of Fig. 9, where the obstacle is engulfed almost symmetrically by the flow. The weak shock detaches without any disturbance. In the other experiments presented in Fig. 10 the flow is non-symmetrical and oblique to the plate, so that it is deflected by the plate, resulting in a stronger reflected shock, which detaches before the flow becomes sonic. It weakens with increasing distance to the plate, but it also accelerates due to the further decrease of the lab-frame flow Mach number. Finally it reaches an almost constant velocity, but the whole trace of the reflected shock in the x, t-diagram is shifted to the left due to the premature shock detachment, so that x_{ll} is underestimated. Schlieren images clearly show the improvement achieved by the needle rakes compared to the thin plate. They produce nearly no disturbance (Fig. 11, right hand side) and allow the passage of whole transverse waves (Fig. 12).

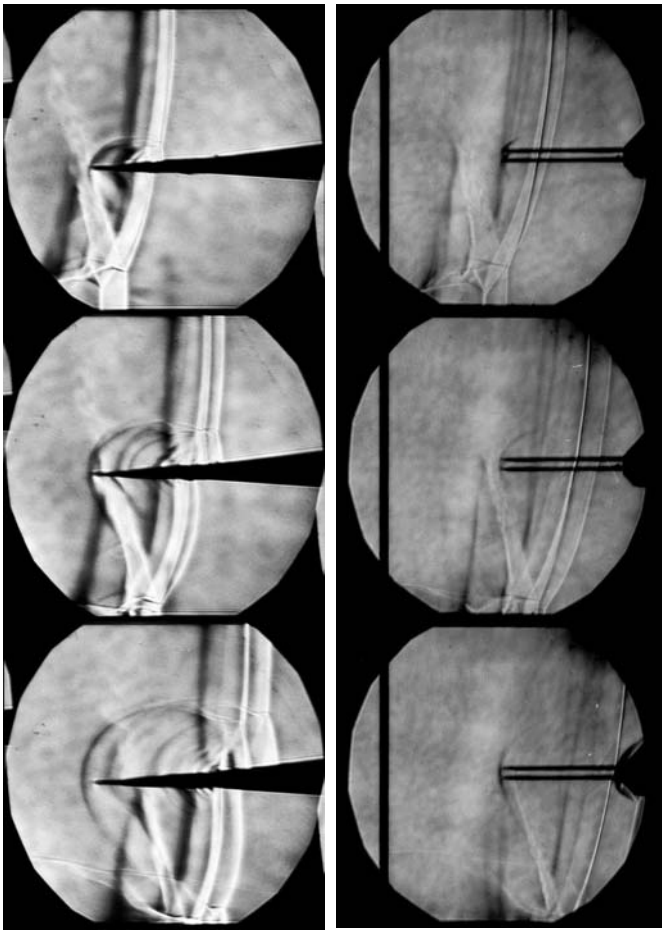

Fig. 11. Oblique flow impinging on the plate and the double rake, $2H_2$+O_2+2Ar, $p_1 = 3.5$ kPa, $\lambda = 108$ mm, $\Delta t = 5$ μs

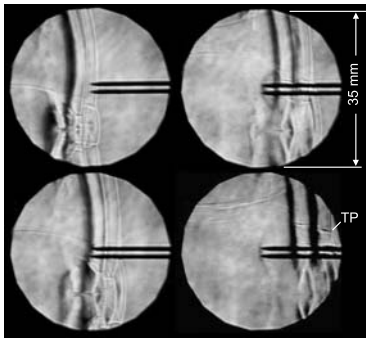

Fig. 12. Transverse wave passing through the double rake, $2H_2 + O_2 + 2Ar$, $p_1 = 5.8$ kPa, $\lambda = 38$ mm, $\Delta t = 2.5$ μs

A disadvantage of the sharp needle rakes has been found by use of shock waves in nitrogen with post-shock Mach numbers (lab-frame) corresponding to those of post-detonation wave conditions. The linear fits through the reflected shock positions in the x, t-diagram do not originate from the needle tips, but from a position about 0.5 mm downstream of them, i.e. the reflection is delayed. This observation is interpreted as follows. The tip itself represents too small an obstacle for the reflected wave to become visible. For single rows of sharp needles in experiments no reflection is observed either, so that the pressure gradient that deviates the flow to the free space on either side of the row seems to be still low. For the double and triple rakes now, the flow cannot directly escape to the side, when the single weak shocks meet each other between the rows, so that a stronger, visible effect appears at that time. The reflection delay $\Delta x_{0,n}$ can be larger with other arrangements of sharp needles. For detonation waves with very large structures the effects produced by the single needles merge faster than the conditions of the incoming flow change, so that a joint reflected shock is already established, when the (lab-frame) sonic surface arrives, but at small scale the delay leads to an overestimation of the wave thickness of up to $\Delta x_{0,n} \cdot (1 + D/v_r)$.

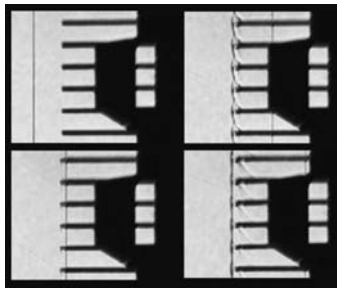

Fig. 13. Reflection of shock wave from a blunt needle plane (edges vertical, $M_2 = 1.01$, BR = 0.019, N_2, $\Delta t = 10\mu$s)

To increase the reflection efficiency of the tips, these have been shortened and provided with blunt wedge tips as indicated in Fig. 8. The distances between the needles have been increased to reduce the blocking and the needles were arranged in a plane covering the whole cross-section to promote a more one-dimensional motion of the reflected shocks and to see a larger number of effects simultaneously. Shock wave experiments with this set-up revealed a better behavior of the reflected shock accompanied by a visible upstream shift of the foot point, $\Delta x_{0,n}$, that now ranges from -0.3 to 0.4 mm. This is still not very satisfying as far as the accuracy of small scale experiments is concerned, but it is an improvement. The relative Mach numbers of the reflected shock range from about 1.01 for $M_2 = 0.75$ to only 1.08 for the most sensitive case of $M_2 = 1.0$. Figure 13 shows the first frames of an experiment for the latter case.

The results of hydrogen-air detonations given in Fig. 14 show, that the mean shock detachment from the needle plane is more regular than with the thin plate (Fig. 10), and thereby closer to the expected behavior (see Fig. 4); and that a higher blockage ratio (3 against 4.5 mm needle spacing) results in just slightly larger reflection velocities (strengths).

For needle planes, a strong reflection of the detonation wave from the mounting plate can hardly be avoided. This wave closes up to the weak reflected wave under investigation and shortens the useful observation time, which, at large scale, decreases somewhat the accuracy of the determined reflection velocity and influences x_{ll} (Eq. 4). To extend the useful time interval, for future studies it is sug-

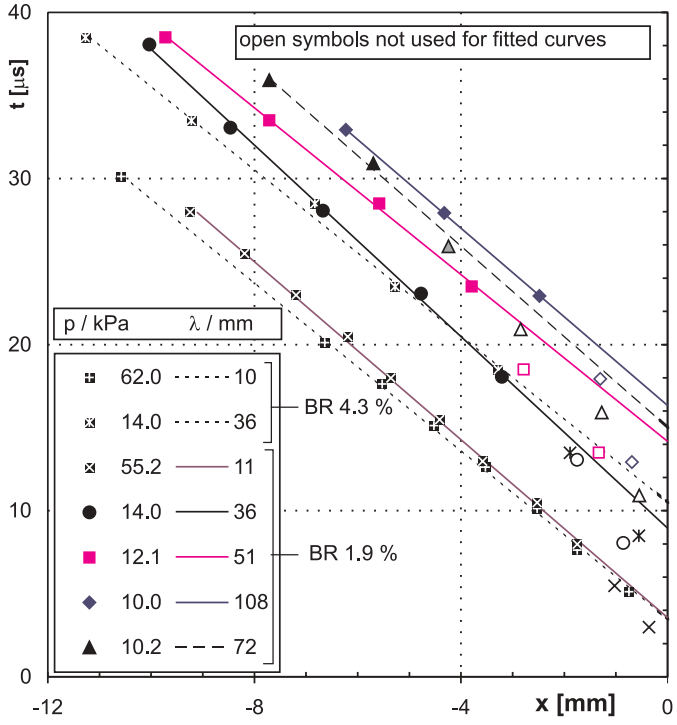

Fig. 14. Waves reflected from bluntly wedged needle planes (H_2-air, including experiments of Figs. 15 to 18)

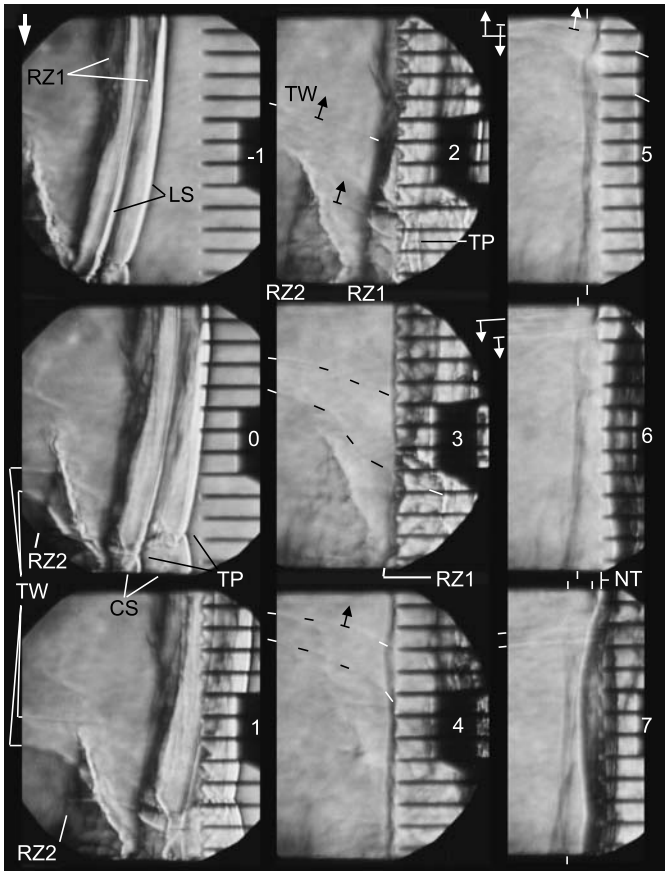

Fig. 15. Reflection of marginal detonation wave at a needle plane (H_2-air, $p_1 = 10$ kPa, $\lambda = 108$ mm, $\Delta t = 5\mu$s, spacing = 4.5 mm, blur of the needle tips NT caused by high optical sensitivity)

gested to use longer needles and to perforate the mounting plate as much as possible.

6 Details of shock detachment and sonic transition

The uniform distribution of obstacles over the whole cross section allows in fact a more detailed observation of the detachment process and of the reflected shock, if structures are large enough. Therefore, in this section observations for marginal detonation waves are discussed. Figure 15 shows such a wave propagating in hydrogen-air. The blur of the needle tips is caused by the high optical sensitivity. Frame[2] "−1" shows mainly two leading shock waves LS followed by two reaction zones RZ1 (dark), which are partially outshined by the white schlieren effect of the curved parts of the shock waves (see Sect. 3). A transverse wave reflection has just occurred at the lower wall on frame −1. The endpoints TP of the upwards running shock triple-line are visible up to frame 2. The corresponding transverse wave TW traverses for the second time an "old" reaction zone RZ that once belonged to the just vanished leading shock. Its remains vanish after frame 3, too. A contact surface CS is formed at the triple-line (better visible on Fig. 16). Single oblique shock-waves are visible at each needle tip on frames 1 to 3, indicating supersonic flow. On frame 4 they have already merged and started to detach – preferably in the lower region where the transverse wave has already passed. Reflected shock wavelets[3] can be distinguished on frames 5 to 7. The short vertical white lines indicate their estimated mean position. At the upper shock tube wall the detachment is delayed till the just reflected transverse wave has passed again (frame 6), which occurs before the wave reflected from the mounting plate arrives. On frame 7 it is about two millimeter apart from the needle tips NT.

These observations seem to correlate well with the increase of the speed of sound through compression by the transverse wave. But, in another experiment under the same initial conditions and in a very similar flow situation, the transverse wave instead seems to push the already detached shock back to the needle tip (Fig. 16). On frame 4 the shock has already detached, but after the transverse wave reflection, two frames later, there is again a quite strong shock attached to the uppermost needle, while only a small sign of a detached shock appears 2 mm upstream of it - probably in another depth of the flow field with slightly different flow conditions. On frame 7 the obstacle shock starts to detach again - although very slowly. And

[2] Positive frame numbering begins always, when the front has just passed the obstacle

[3] The terminus wavelet refers to the visible single parts of a wavy shock wave that move in different depths of the flow field.

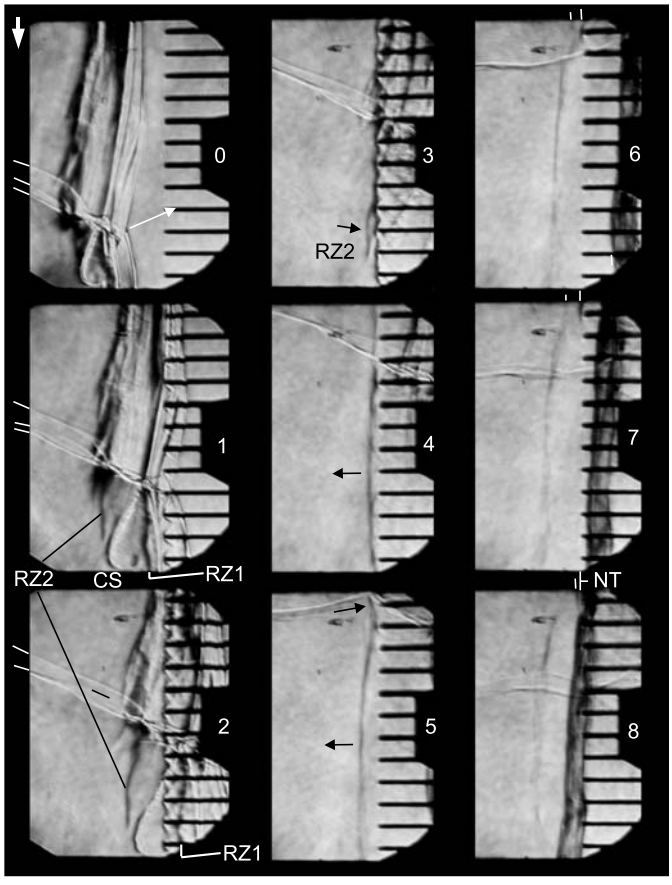

Fig. 16. Effect of transverse wave and reaction zone on shock detachment (same initial conditions as Fig. 15, but $\lambda = 72$ mm)

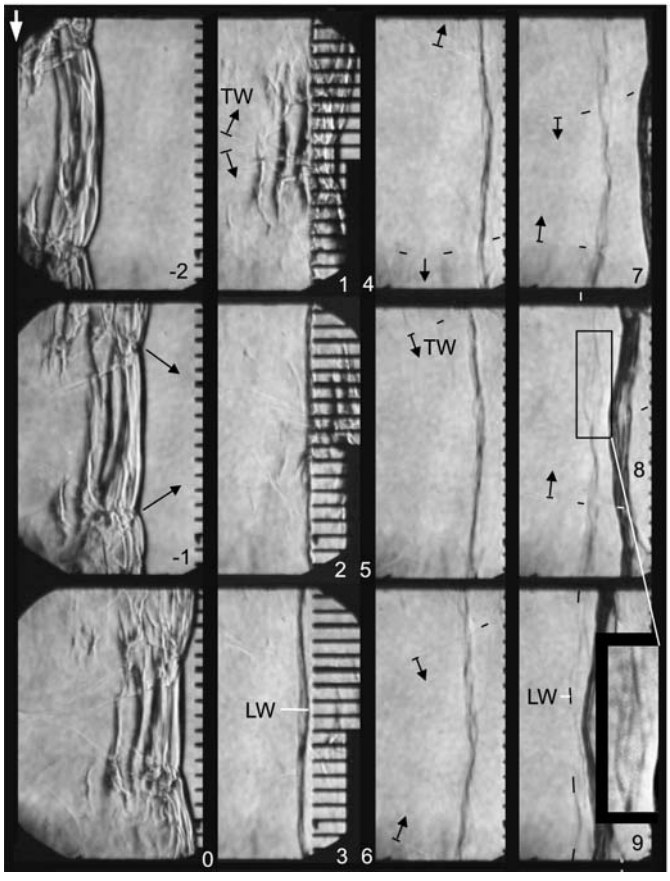

Fig. 17. Large fluctuation of wavelet movement (H_2-air, $p_1 =$ 14 kPa, $\lambda =$36 mm)

this relatively slow motion of the upper wavelet is also observed for the last discussed experiment (Fig. 15, frames 6 to 7). This means, that the effect of transverse waves on the shock detachment is not trivial; for the flow situation shown it is rather delaying than accelerating. The angle of the transverse wave at the time of interaction with the obstacle shock should be important, but here it cannot be the reason for the somewhat different observations, because in Fig. 15 the mean angle for the two waves is even slightly smaller than in Fig. 16.

Some obvious differences of the flow situation of Fig. 16 in respect to that of Fig. 15 are the longer distances that the Mach stems (lower front shock waves) have already covered — measured from their points of origin, when they start to interact with the obstacle, the smaller difference between the Mach stem velocities, the presence of three transverse wavelets (frames 0 to 2), and tracks of a third, weak transverse wave in the soot pattern taken 140 mm in front of the needles. While the first difference might correlate with the different observations at the upper needle, the others indicate that in Fig. 16 there are two transverse waves moving in the horizontal plane in opposite directions. These cause that the front waviness in the line of sight is lower than in Fig. 15. This allows a detailed observation of the contact surface CS, which is rolling up seemingly undisturbed by the wall boundary layer, and of the following older reaction zone RZ2, that seems to have an important role in the detachment process. The fast shock waves of the lower detonation wave segment - under the transverse wave - and their corresponding reaction zones RZ1 have passed the obstacle plane on frame 2, but the flow is still supersonic. The obstacle shock does not detach before RZ2 passes the obstacles (frame 3), and then the weak shock moves upstream very fast. In Fig. 15 the fast detachment in the lower third of the flow field between frames 3 and 4 does also seem to be correlated to the second traverse of a reaction zone in frame 3 (RZ1). And maybe even the old reaction zone RZ2 that vanishes in frame 3 contributes to the increase of the shock velocity towards the lower wall. It is not yet understood why the delay at the upper wall in both experiments is almost sharply limited to a region of about 5 mm height.

A number of experiments indicate, that the detachment is delayed or its velocity is reduced behind those sections of the front that have already propagated more than half of a cell length, when they touch the needle tips (Figs. 15 to 19). These at last or slowly detaching wavelets do not quickly catch up with the others. While for $\lambda = 2d$ they do not do it within the observation time, for $\lambda \leq d$ (Figs. 17 and 18) it can be observed that they finally overtake the others. In Fig. 17 it takes about 35 μs till the latest detached wavelet LW takes the leading po-

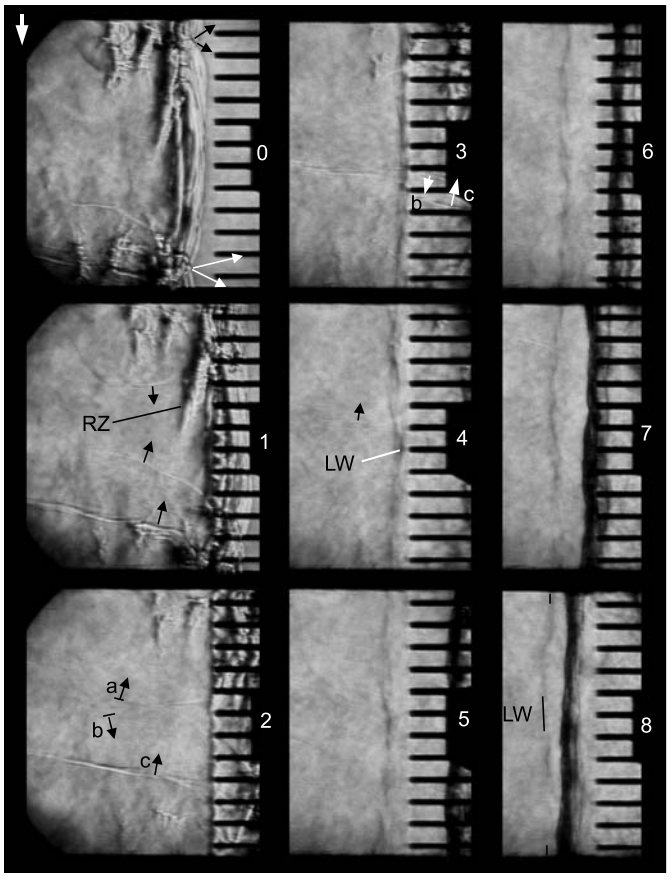

Fig. 18. Small fluctuation of wavelet movement (H_2-air, $p_1 = 14$ kPa, $\lambda = 36$ mm)

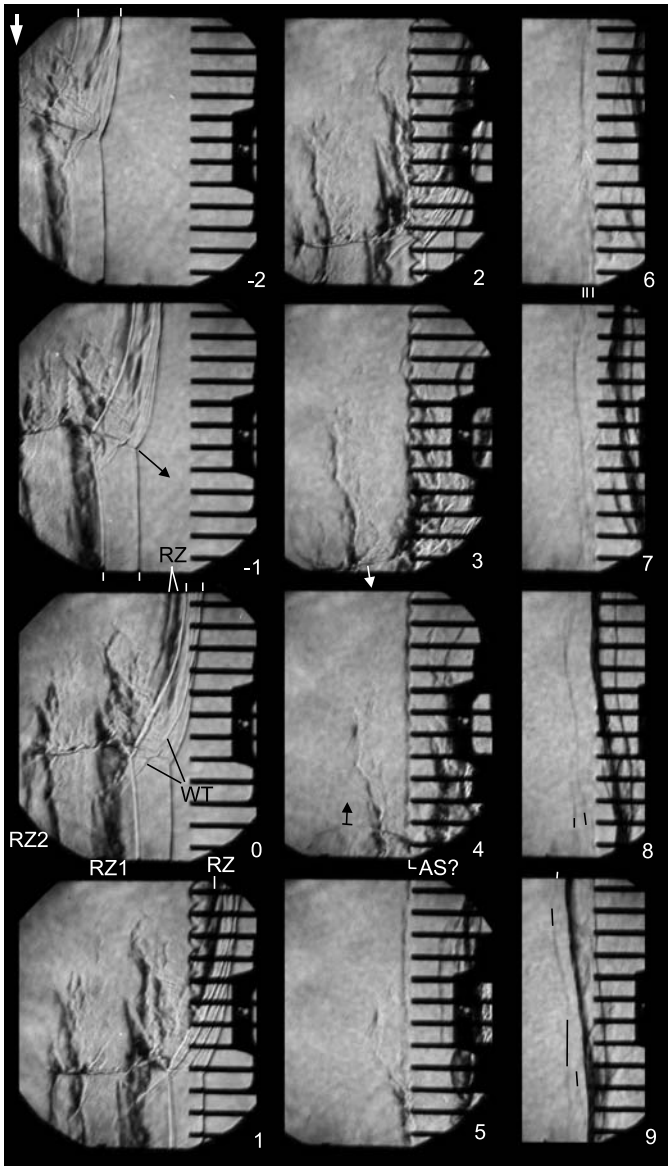

Fig. 19. Effects of three-dimensionality and locally overdriven state (C_2H_2-air, $p_1 = 7$ kPa, $\lambda = 89$ mm)

sition (frames 2 to 9). Figure 18 shows a situation where transverse wave reflections at the walls occurred around the obstacle position, i.e. the front segment in the middle of the tube has passed *about* half of a cell at the time of contact. The weak shock detaches first in the middle (frame 2). Then it faces the transverse waves "a" and "b". Again these decelerate the detachment, so that the middle section moves slower than the other parts - especially than the lower one (3, 4). Later it leads again (8). The way from the rearmost to the foremost position took about 20 μs, i.e. less than in the first case. These times are close to the initially mentioned characteristic time λ/a_{ss}, that is 34 μs here.

Frame 8 of Fig. 17 shows the widest distance between wavelets that was observed in this work (~ 6 mm).

Effects of pronounced three-dimensionality on the sonic transition are discussed based on Fig. 19. The wavy shock front appears in form of two separated thin lines, because the curved shock wave surface linking them has not a sufficient integrated schlieren effect[4]. In such a flow situation, where there is only one strong transverse wave moving in the direction of the optical axis, the visible parts of the front shock wave surface are moving each along one of the window surfaces. To check this one may imagine to watch the foremost line in the vertical direction (frames $-2, -1$). That the second line appears bright, indicates that it has a low depth in the line of sight.

The two dark vertical schlieren areas RZ1 and RZ2 moving along the lower wall are reaction zones. To evaluate the detachment process it is important to know to which shock wave each of them belongs. The distance between the two lower segments of the shock front surface slightly decreases with time, so that the second line must be the Mach stem in the horizontal plane, like it is obviously the case for the upper segments. This is in accordance with the observation from the soot pattern, that the wave is in a rectangular mode. As the induction distance behind the faster of the lower wave segments *cannot* be longer than that behind the slower one, and the distance between the second segment and RZ2 *is* longer than that

[4] The optical sensitivity was lower than in Fig. 15 (see Sect. 3).

between the first segment and RZ1, it is not probable that RZ2 is the reaction zone that belongs to the lower part of the second line. That one must be a part of the schlieren area RZ1. RZ2 then consists of the remains of an "old" reaction zone, i.e. the one that once belonged to the leading shock that has vanished with the last wall reflection of the horizontally moving transverse wave. As the last but one reflection had occurred at the rearward wall of the shock tube at about the end of the sooted plates, that are located 93 mm in front of the beginning of the visible area, the *last* reflection must have occurred just in front of this area. This consideration is supported by the vanishing of the old reaction zone RZ2, observable up to frame 6. RZ1 does not seem to vanish at the same rate.

Immediately after contact of the first segment of the lower leading shock wave with the obstacle the bow shocks are hardly visible, they appear only when the whole shock front has passed (frame 2). The transition from supersonic to subsonic occurs rapidly between frames 2 and 4 during the traverse of the corresponding reaction zones RZ1. On frame 4, above of the just reflected transverse wave, the shock looks detached already, although RZ2 has not yet arrived, whereas *under* the transverse wave the obstacle shock seems to be attached. After RZ2 has passed the needle tips, three wavelets can be identified in front of the lower needles (frame 6). Two wavelets detach — probably in those depths of the flow field that are traversed by RZ2, but the third stays close to the obstacles till on frame 9 it is absorbed by the wave reflected from the mounting plate.

The upper detonation wave segments, above of the transverse wave, have passed about 40 % of a cell length, when they reach the obstacle plane. Between the two strong lines, a third, weak line is observed (WT) that indicates a second, weak transverse wave[5]. One trace of such a wave appeared as well on the soot track (not two). An impact on the shock detachment is not observed. The rearward upper shock wave segment does close up quickly to the leading segment and has nearly reached it at the obstacle position. While on frame -1 it is immediately followed by a reaction zone, on frame 0 two de-coupled reaction zones are observed. Visible effects of the reaction zones RZ have just passed the obstacle on frame 1, but the flow remains supersonic. This correlates with the overdriven state of the faster wave segment — $D^2_{\mathrm{loc}}/D^2_{CJ} = 1.49$ between frames -2 and 0. For the other segment this value is 0.86, so that the flow Mach number must be smaller than the C-J value, but an associated effect (detaching shock) is not visible. Again, the detachment of the shock, observable from frame 4 on, seems to be correlated to the traverse of reaction zones that belong to older wave segments (RZ1, frame 3). It starts slightly later than in the lower region, but then the upper wavelets move faster upstream. The lower ones do not close up (following frames). Where RZ1 is not visible and probably not present, directly adjacent to the upper shock tube wall, the detachment is delayed as well.

[5] The main triple line cannot overtake the rearward front shock wave.

Generally it is observed that the curvature or waviness of the weak reflected shock is clearly smaller than that of the detonation front, but this does most probably not apply to the curved (instantaneous) sonic surfaces. The lab-frame ones could possibly be reconstructed on the basis of a large number of experiments in a flat channel, that provides a more unambiguous and repeatable, two-dimensional flow. The local detachment times have to be measured more exactly as well, because small errors have an enormous effect on the distance to the detonation wave front. So, here a reconstruction of the sonic surfaces is not appropriate. The average ratio of curvatures between the lab-frame sonic surface and the reflected shock is presumably about $D/v_r \approx 5$.

While the location of the sonic plane as defined in Sect. 1 is determined approximately by the x,t-point where the average velocity of the reflected shock becomes nearly constant, this is not true for single wavelets, i.e. they might propagate temporarily at a constant velocity, but that does not indicate a local equality of the speed of sound a and the particle velocity u in the detonation wave frame. Also the local equality of the wavelet velocity with a theoretical value $M_r a_{ss} + a_{ss} - D$, where M_r is the reflected shock Mach number (close to 1), would not indicate the presence of a fragment of the instantaneous shock-frame sonic surface as defined in section one, but just $u_{local} = a_{ss}$. In this work the reconstruction of such a surface is refrained, because of two reasons. First, the temporal and optical resolution are again not sufficient, and second, the observed fluctuations of the wavelet velocities increase the probability that local sonic transitions repeatedly appear downstream[6] of the sonic plane, so that the mean location of the (instantaneous) sonic surfaces will also be downstream of the sonic plane. And the determination of the latter is of larger practical importance because of its use in stream tube deficit models.

7 Velocity of the reflected wave

The observed velocities of the reflected wave are shown in Fig. 20 in comparison to experimental data reported by Vasiliev (1973) and by Gvozdeva (1986), and to three theoretical estimates. Vasiliev used a thin plate obstacle and streak schlieren photography. He chose to plot the results over d/λ and obtained a common curve for various mixtures, that were quite similar to those in use here (+ methane-oxygen and argon diluted acetylene-oxygen, no fuel-air), and his curve is somewhat above of the results of this work. The kind of obstacle does not serve to explain this discrepancy, because the very different obstacles of this work do not exercise such a significant influence on the reflection velocity. Just the two thin plate results for pure oxy-hydrogen are located somewhat above those obtained with other obstacles, but this is due to the already mentioned mixture richness in that case. Gvozdeva's experiments have been performed with a bursting diaphragm followed by air that ostensibly produced an expansion wave.

[6] in shock-fixed co-ordinates

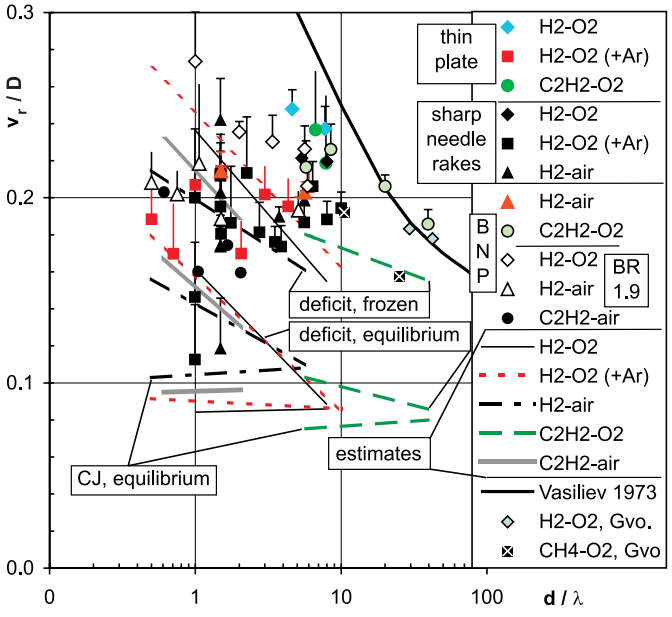

Fig. 20. Experimental reflection velocities compared to data of Vasiliev (1973) and Gvozdeva (1986), and to theoretical estimates, based on C-J theory values for given initial pressures (lower ones), on Eq. (7) using the measured detonation velocity D (intermediate ones), and on Eq. (8) using D and wave propagation at a_f. (BNP = blunt needle plane, +Ar = 40 % Ar, measurement uncertainties valid for both directions)

Her hydrogen results fit Vasilievs curve, the methane results are lower. All experimental results, including the present ones, have in common that the reflected waves are clearly faster than equilibrium sound waves propagating upstream under C-J conditions at the given pressure (Fig. 20).

For a self-sustained detonation wave ($u_2 = a_2$) under deficit conditions, the reflection velocity is estimated by use of the energy equations for the C-J wave and for the real (experimental) wave, and an integrated differential expression for the real sonic state enthalpy (see Sect. 1). Sound speeds are based on equilibrium chemistry.

$$\begin{aligned}
\frac{D_{CJ}^2}{2} + h_1 &= \frac{a_{CJ}^2}{2} + h_{CJ}\,, \\
\frac{D^2}{2} + h_1 &= \frac{a_{ss}^2}{2} + h_{ss}\,, \\
h_{ss} - h_{CJ} &= c_{p,e}(T_{ss} - T_{CJ}) - \Delta h^R \beta_{ss} \\
&= \frac{a_{ss}^2 - a_{CJ}^2}{\gamma_{e,CJ} - 1} - \Delta h^R \beta_{ss}\,.
\end{aligned}$$

These equations yield a_{ss} as function of the measured wave velocity D and the non-equilibrium parameter β_{ss}:

$$0 = D_{CJ}^2 - D^2 + \frac{\gamma+1}{\gamma-1}\,(a_{ss}^2 - a_{CJ}^2) - 2\Delta h^R \beta_{ss}\,. \qquad (6)$$

To obtain the reflection velocity, here, β_{ss} is set to zero, because reliable expressions for the relaxation and the boundary layer displacement have not yet been found.

$$v_{r,e} = a_{e,ss} - (D - u_{ss}) = 2a_{e,ss} - D\,. \qquad (7)$$

For $\beta_{ss} > 0$, a_{ss} and thereby v_r would be somewhat smaller. Equation (6) shows that a velocity deficit, i.e. a decrease of D, leads just to a relatively slight decrease of a_{ss} (low value of γ_e) and thereby to an increase of the reflection velocity v_r. This tendency is shown by the linear fits inserted in Fig. 20. The single values are not shown to keep the diagram readable. For higher order fits the number of data points is not sufficient. The upper estimate, for wave propagation at the sound speed for frozen chemistry and vibration, is based on the latter estimate and an assumed constant ratio a_f/a_e:

$$v_{r,f} = a_{f,ss} - (D - a_{e,ss}) = a_{e,ss}\left(\frac{a_{f,CJ}}{a_{e,CJ}} + 1\right) - D\,. \qquad (8)$$

As mentioned at the end of Sect. 1, it is not known, wether the observed schlieren effect belongs to the head of the weak reflected wave, that moves at a_f but decays in strength, or its main part moving at a_e. The observed, quite abrupt endings of the reaction zones indicates rather fast chemistry and therefore equilibrium propagation.

Practically, the mentioned tendency is observed for the experiments with the blunt needle planes and for the pure fuel-oxygen mixtures, as well as for the referenced results, but fuel oxygen mixtures yield values are even clearly above the upper estimates. Hydrogen air results are more or less in agreement with Eq. (8), and acetylene-air results are in between the equilibrium and the frozen estimate. Only the experimental velocities for Argon diluted hydrogen-oxygen and hydrogen-air obtained with sharp needles do not show a clear tendency. Their values scatter around $v_r/D = 0.2$. Occasional extraordinary low values from sharp needle experiments at low pressures correlate with early fading of the waves, that has been observed in these cases.

Up to now there is no satisfying explanation for the discrepancies between the estimated and the observed reflection velocities. One might suppose that the reflection was stronger than a sound wave, but for needle rakes and thin plates the wave strength would decrease quickly with distance from these single obstacles, so that the reflection velocity would become lower than in the case of a needle plane that covers the whole cross section — and this is not observed. Furthermore, for flow Mach numbers[7] behind the wave of less than 0.86, which are valid for the detonative mixtures studied, experiments with shock waves in nitrogen reflecting at the blunt needle planes yielded reflected shock Mach numbers of less than 1.03. This value can only account for a fraction of the discrepancy.

8 Lower limit for the wave thickness

Figure 21 shows the lower limit values from the plate experiments over the cell size in comparison to those of

[7] in the lab-frame

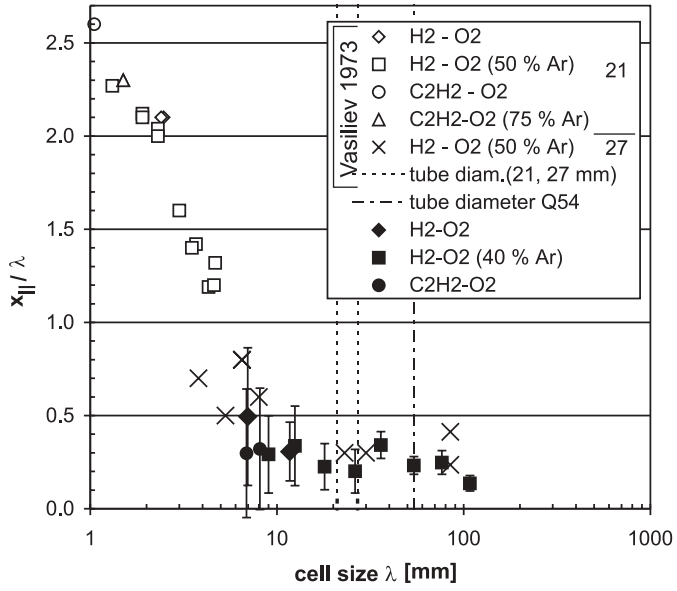

Fig. 21. Lower limit of the wave thickness obtained by thin plates. Error bars according to Eq. (4)

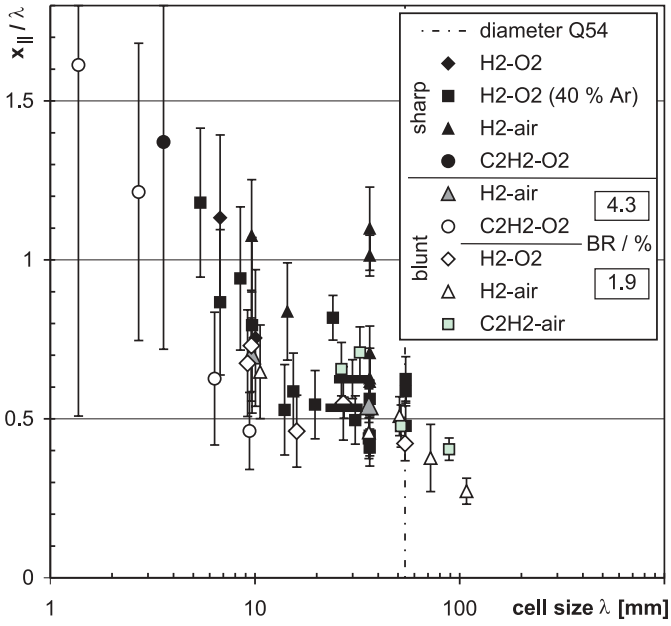

Fig. 22. Lower limit of the wave thickness for different needle arrangements. Thick horizontal bars indicate average results obtained with sharp needle rakes and blunt needle planes for hydrogen mixtures with cell sizes between 9 and 54 mm

Vasiliev et al. (1972a and b). The error bars show the estimated maximum statistical error according to Eq. (4), which must increase for smaller scales. Within the common range of cell sizes ($\lambda > 7$ mm) the present values are slightly smaller than those of Vasiliev, which reflects the differences in the evaluation method as explained in Sect. 2. The steep increase of the length ratio towards small scale observed by Vasiliev is also partially due to the evaluation method. If the results were plotted over λ/d, the small tube results would shift to the right relatively to the large tube ones — to a degree that corresponds to the distance of the vertical lines. This shows that a unique correlation between both ratios, which was proposed by Vasiliev et al. (1972a) based on the small tube results only, does not exist.

As expected, the relative lower limit values obtained with needle arrangements (Fig. 22) are clearly larger than the thin plate values. To compare the different needle arrangements the results for hydrogen mixtures may be considered. As expected, especially at small scale the *blunt* needle plane values are lower than those obtained with the *sharp* needle rakes. They also spread less. Though this comparison uses pure oxy-hydrogen results on one side and such of argon-diluted oxy-hydrogen on the other, however Figs. 21 and 22 show that the results for both mixtures do not differ significantly, when the same obstacle is used. The two different blunt needle planes give essentially the same results. Average ratios of the lower limit value to the cell size of all experiments with hydrogen are obtained in the medium cell size range from 9 to 54 mm by weighting each value with the inverse of the estimated accuracy. For blunt needle planes it is 0.54 with a standard deviation of 0.03, for sharp needle rakes 0.63 ± 0.06.

For small cell sizes, the ratio of the lower limit value to the cell size increases, although to a lesser extend than in Vasiliev's plate experiments. The authors have no satisfactory explanation for this observation so far, because the systematic error due to the waviness of the front should only account for a small fraction of the effect (< 0.2). An increase of the relative distance of the *shock* frame sonic plane versus small values of λ/d can be explained by the low relative area expansion and Eq. (2), but the lab frame sonic transition and the lower limit value should not be affected.

With increasing marginality, $\lambda > d$, the relative lower limit value decreases. This can be explained by the fact that the post-wave flow becomes more and more subsonic (in the laboratory frame) as the deficit of the wave velocity increases, so that the location of the lab frame sonic plane shifts towards the front.

9 Conclusion and outlook

The reflection of detonation waves from slight obstacles has been studied for a variety of mixtures, initial pressures and obstacle types. Measurement details, error sources and obstacle influences have been analyzed. An arrangement of bluntly wedged needles in a plane covering the whole cross section such that their tips face the detonation wave and the blockage ratio is low (< 2 %) turned out to be the most suitable obstacle type. The optimum size and spacing of the obstacles to generate a sudden small flow disturbance with a sufficient schlieren effect depends on the C-J state density and on the wave thickness and has to be found still. Important observations are the initially strongly supersonic flow behind overdriven wave segments, a detachment promoting effect of "old" reaction zones — especially where they follow the overdriven wave segments,

a non-trivial sometimes detachment delaying role of the transverse waves, and the fluctuating motion of reflected wavelets downstream of the sonic plane, whose period is of the order of λ/a_{ss}. In the medium range of cell sizes, that offers a reasonable measurement accuracy ($\lambda \geq 9$ mm), and that does not yet produce too strong velocity deficits ($\lambda \leq d$), the evaluation yielded a lower limit value for the detonation wave thickness of 0.4 to 0.8 times the cell width. In this range, the wave thickness roughly equals one cell width. The observed reflection velocities are smaller than referenced data, but larger than those of equilibrium sound waves — even when the effect of the velocity deficit on the sonic state is considered. Anyhow, most mixtures show roughly the estimated tendency of the deficit effect.

The method is especially suitable to study the structure of detonation waves in mixtures with large cellular structures and large densities (e.g. fuel-air), which yield large schlieren effects. For mixtures with very irregular, and multi-scale structures or for studies at elevated initial temperatures, where soot track quality deteriorates, it might deliver better defined data than the soot track method.

For future work it is suggested to determine the mean trajectory of the reflected shock and especially the course of its acceleration more exactly by use of a larger number of experiments per condition, and to compare these to theoretical estimates based on relaxation laws and validated boundary layer models. The obstacle has to be designed in such a way that the reflected shock reaches a stable strength clearly before it crosses the path of the (shock frame) sonic plane. The location of the latter is obtained then by the point where the acceleration of the weak shock decreases under the estimated, corresponding small value. To improve velocity deficit models any further, also the measurement of the detonation wave velocity has to be very accurate (error < 1 %).

Acknowledgements. The financial support of the Deutsche Forschungsgemeinschaft (DFG) under grant number OL 107/4-1,2 is gratefully acknowledged. The authors thank F. Zhang for a thorough discussion on basic principles, and A.A. Vasiliev and S.B. Murray for kindly mailing their reports on the topic.

References

Auffret, Y., Desbordes, D., Presles, H.N.: Detonation structure and detonability of $C_2H_2 - O_2$ mixtures at elevated initial temperature. Shock Waves **11**, 89–96 (2001)

Barthel, H.O.: Predicted spacings in hydrogen-oxygen-argon detonations. Phys. Fluids **17**(8), 1547–1553 (1974)

Bull, D.C., Elsworth, J.E., Shuff, P.J.: Detonation cell structures in fuel/air mixtures. Combust. Flame **45**, 7–22 (1982)

Dabora, E.K., Nichols, J.A., Morrison, R.B.: The influence of a compressible boundary on the propagation of gaseous detonation. *10th Symp. (Int.) on Combustion*, pp 817–839. The Combustion Institute, Pittsburgh (1965)

Desbordes, D.: Transmission of overdriven plane detonations: Critical diameter as a function of cell regularity and size. Progress in Astronautics and Aeronautics **114**, 170–185 (1988)

Desbordes, D.: Aspects stationnaires et transitoires de la detonation dans les gaz: relation avec la structure cellulaire du front. PhD thesis, Universite de Poitiers (1990)

Edwards, D.H., Parry, D.J., Jones, A.T.: The structure of the wave front in spinning detonation. J. Fluid Mech. **26**, 321–336 (1966)

Edwards, D.H., Jones, A.T., Phillips, D.E.: The location of the Chapman-Jouguet surface in a multi-headed detonation wave. J. Phys. D **9**, 1331–1342 (1976)

Edwards, D.H., Hooper, G., Morgan, G.M., Thomas, G.O.: The quasi-steady regime in critically initiated detonation waves. J. Phys. D **11**(13), 2103–2117 (1978)

Fay, J.A.: Two-dimensional gaseous detonations: velocity deficit. Phys. Fluids **2**, 283–289 (1959)

Gvozdeva, L.G.: Unsteady interaction detonation waves. In: Korobeinikov, V.P. (ed) *Unsteady interaction of shock and detonation waves in gases,* p. 175. (1986) Engl. ed. by Urtiev PA, Hemisphere, New York 1989

Hartunian, R.A., Russo, A.L., Marrone, P.V.: Boundary-layer transition and heat transfer in shock tubes. J. Aerospace Sci. **27**, 587–594 (1960)

Laberge, S., Knystautas, R., Lee, J.H.S.: Propagation and extinction of detonation waves in tube bundles. Prog. Astronautics and Aeronautics **153**, 381–396 (1993)

Murray, S.B., Lee, J.H.: The influence of physical boundaries on gaseous detonation waves. Progress in Astronautics and Aeronautics **106**, 329–355 (1986)

Reynolds, W.C.: *The Element Potential Method for Equilibrium Analysis: Implementation of the interactive program STANJAN,* Version 3. Stanford University 1986

Strehlow, R.A.: Transverse Waves in Detonations: II. structure and spacing in H_2-O_2, C_2H_2-O_2,C_2H_4-O_2, and CH_4-O_2 systems. AIAA J. **7**(3), 492–496 (1969)

Soloukhin, R.I.: Nonstationary phenomena in gaseous detonation. *12th Symp. (Int.) on Combustion,* pp 817–839. The Combustion Institute, Pittsburgh (1969)

Vasiliev, A.A., Gavrilenko, T.P., Topchian, M.E.: On the Chapman-Jouguet surface in multi-headed gaseous detonations. Astron. Acta **17**, 499–502 (1972a)

Vasiliev, A.A., Gavrilenko, T.P., Mitrofanov, V.V., Subbotin, V.A., Topchian, M.E.: Location of the sonic transition behind a detonation front. Combust. Explos. Shock Waves **8**, 98–104 (1972b)

Vasiliev, A.A.: Chapman-Jouguet condition for real detonation waves. Combust. Explos. Shock Waves **9**, 309–315 (1973)

Vincenti, W.G., Kruger, C.H. Jr.: *Introduction to physical gas dynamics.* Wiley, New York 1967

Weber, M., Olivier, H., Grönig, H., Biegling, J.: On the location of the Chapman-Jouguet surface in gaseous detonations close to the limit of propagation. *18th Int. Colloquium on Dynamics of Explosions and Reactive Systems*, p. 156. Seattle (2001a) ISBN 0-9711740-0-8

Weber, M., Olivier, H., Grönig, H.: Propagation mode of detonation waves in narrow gaps. In: Lu, F.K. (ed.) *23rd Int. Symp. on Shock Waves*, p. 3212. Fort Worth (2001b) ISBN 0-9721227-0-2

Williams, F.A.: *Combustion theory*, 2nd ed, p 35. Addison-Wesley, New York 1985

Zitoun, R., Desbordes, D., Guerraud, C., Deshaies, B.: Direct initiation of detonation in cryogenic gaseous H_2-O_2 mixtures. Shock Waves **4**, 331–337 (1995)